Orientation of the Oxygen-Evolving Manganese Complex in a Photosystem II Membrane Preparation: An X-ray Absorption Spectroscopy Study†

Ishita Mukerji,‡,§ Joy C. Andrews,§,∥ Victoria J. DeRose,§,⊥ Matthew J. Latimer,§,∥ Vittal K. Yachandra,*,∥ Kenneth Sauer,*,§,∥ and Melvin P. Klein*,∥

Department of Chemistry and Structural Biology Division, Lawrence Berkeley Laboratory, University of California, Berkeley, California 94720

Received November 16, 1993; Revised Manuscript Received June 1, 1994®

ABSTRACT: X-ray absorption spectroscopy has been performed on oriented photosystem II membrane particles isolated from spinach. Structural features of the tetranuclear Mn cluster and the orientation of the cluster with respect to the lipid bilayer were determined in both the S_1 and S_2 states of the Kok cycle. Variation of the sample orientation with respect to the X-ray e-vector yields highly dichroic K-edge and extended X-ray absorption fine structure spectra (EXAFS), indicative of an asymmetric tetranuclear cluster. Mn–Mn vectors at 2.72 and 3.38 Å can be resolved from these measurements using quantitative analysis. The 2.72-Å vector, consisting of at least two component vectors, is oriented at an average angle of 60° ± 7° to the membrane normal, with an average of 1.1 ± 0.1 interactions per Mn atom. The 3.38-Å vector, most probably an average of two vectors, makes an angle of 43° ± 10° with respect to the membrane normal, with an average of 0.45 ± 0.07 backscatterer per Mn atom. Upon advance to the S_2 state, the orientation of these vectors and the average numbers of backscatterers are approximately invariant. Analysis of more subtle features of the EXAFS reveals changes accompanying this S-state advance that are consistent with the oxidation of Mn during this transition. However, the dominant structural features of the oxygen-evolving complex remain constant in the S_1 and S_2 states. The structure of the Mn complex and the orientation of the complex in the membrane within the context of dichroism of the X-ray absorption data are discussed.

Photosystem II (PS II[1]) in plants and algae consists of a reaction center, believed to be structurally similar to the crystallographically characterized reaction center of purple non-sulfur bacteria (Deisenhofer et al., 1985; Babcock et al., 1989), and a donor complex that oxidizes water to dioxygen. The catalytic site of the donor complex contains a tetranuclear Mn cluster, which forms the locus for charge accumulation and water oxidation. The energy of four successive photons absorbed by the reaction center pigment P_{680} of photosystem II provides the driving force for the oxygen-evolving complex (OEC) as it cycles through a series of five intermediate S states (Kok et al., 1970). The specific arrangement of electron transfer components within the lipid bilayer facilitates the vectorial transfer of electrons from the Mn donor complex to the acceptor quinones. Thus, spectroscopic studies using oriented membranes shed light on not only the arrangement of the complex with respect to the lipid bilayer but also the symmetry of the complex being studied.

Extensive electron paramagnetic resonance (EPR) and optical studies of oriented bacterial reaction centers led to the successful prediction of the geometric arrangement of the electron transfer components within the membrane, as confirmed by the X-ray crystal structure of the reaction center (Deisenhofer et al., 1985). The orientation of Fe–S centers in photosystem I has also been studied extensively with EPR spectroscopy (Prince et al., 1980; Dismukes & Sauer, 1978; Brettel et al., 1992). Rutherford (1985) presented a systematic study of the various EPR signals arising from oriented PS II membranes, from which the orientation of cytochrome b_{559} and other electron transfer components within the lipid bilayer was determined. X-ray absorption study of oriented membrane preparations is emerging as a powerful method for investigating the symmetry and structure of metalloenzymes (George et al., 1989, 1993; Flank et al., 1986; Smith et al., 1985).

The wealth of information obtainable from spectroscopic studies of oriented membrane preparations provides the impetus for our investigation. In this study, Mn K-edge and EXAFS spectra are used to study oriented PS II membranes. These oriented membrane preparations from spinach (Berthold et al., 1981) consist of the reaction center, containing polypeptides D1 and D2, and all of the electron transfer components associated with the reaction center. The 43- and 47-kDa Chl-containing polypeptides and the 16-, 23-, and 33-kDa extrinsic polypeptides are also contained in this protein complex. The structure and symmetry of the OEC in two of the S states of the Kok cycle, the dark-adapted S_1 state and the S_2 state, are investigated. The use of PS II particles offers the possibility of comparing results from oriented preparations with those obtained using randomly oriented samples (DeRose et al., 1994; DeRose, 1990; McDermott et al., 1988; Yachandra et al., 1987; MacLachlan et al., 1992). Previous X-ray absorption spectroscopy (XAS) studies of PS II particles [reviewed in Debus (1992), Sauer et al. (1992), and Klein et al. (1993)] have identified a 2.7-Å Mn–Mn vector, attributed

† This work was supported by National Science Foundation Grant DMB91-04104 and by the Director, Division of Energy Biosciences, Office of Basic Energy Sciences, Department of Energy, under contract DE-AC03-76SF00098.

* Authors to whom correspondence should be addressed.

‡ Present address: Department of Molecular Biology and Biochemistry, Wesleyan University, Middletown, CT 06459.

§ Department of Chemistry.

∥ Structural Biology Division.

⊥ Present address: Department of Chemistry, Northwestern University, Evanston, IL 60208.

® Abstract published in *Advance ACS Abstracts,* July 15, 1994.

[1] Abbreviations: Chl, chlorophyll; Cyt, cytochrome; EPR, electron paramagnetic resonance; EXAFS, extended X-ray absorption fine structure; MES, 2-morpholinoethanesulfonic acid; OEC, oxygen-evolving complex; PS II, photosystem II; XANES, X-ray absorption near edge spectroscopy; XAS, X-ray absorption spectroscopy.

0006-2960/94/0433-9712$04.50/0

to di-μ-oxo-bridged Mn atoms. More recently, the existence of a 3.4-Å vector has been demonstrated, possibly arising from mono-μ-oxo- and mono- or dicarboxylato-bridged Mn atoms or Mn–Ca interactions (George et al., 1989; DeRose et al., 1994; DeRose, 1990; Yachandra et al., 1993; Penner-Hahn et al., 1990).

Both the Mn K-edge spectra and the extended X-ray absorption fine structure (EXAFS) of the oriented PS II membranes exhibit clear dichroism, indicative of an asymmetric Mn cluster. We use these results to determine the orientation of these vectors with respect to the membrane normal and to investigate the effects on the structure and symmetry of the tetranuclear Mn cluster upon advance to the S_2 state of the Kok cycle. From these measurements, an average angle of 60° with respect to the membrane normal was obtained for the 2.7-Å Mn–Mn vector(s), and an average angle of 43° was observed for the 3.4-Å Mn–Mn or Mn–Ca vectors. The relative orientation of these vectors with respect to the membrane normal remains constant upon advance to the S_2 state, which is suggestive of an overall conservation of structure and symmetry of the OEC. However, the evidence from EXAFS analysis is suggestive of minor structural changes occurring upon the S_1 to S_2 state transition. From the average coordination numbers of the two vectors and their relative orientation, the symmetry of the OEC and its arrangement within the lipid bilayer can be determined.

MATERIALS AND METHODS

Sample Preparation and Characterization. PS II particles were prepared as previously described (Berthold et al., 1981). The membranes were resuspended in 50 mM MES, pH 6.0, buffer containing 0.4 M sucrose and 5 mM $CaCl_2$ and pelleted by centrifugation at 4 °C (39000g, 1 h). One or two drops of 50 mM MES buffer were added to the pellet, and the resulting paste was painted onto Mylar tape. The PS II membranes were dried under a stream of cold N_2 gas at 4 °C in the dark for approximately 1 h, as previously described (Rutherford, 1985); however, EDTA was not added. This process was repeated 5–7 times to generate samples with sufficient concentration for X-ray absorption experiments. Orientation of the samples was assessed using X-band EPR spectroscopy performed with a Varian E-109 spectrometer, a standard TE_{102} cavity, and an Air Products liquid helium cryostat. S_2-state samples were prepared by illumination at 195 K for 5–10 min. The amount of $g = 2$ multiline signal formed was 95–100% of that observed for a regular preparation of unoriented membranes, relative to the iron signal at $g = 4.3$. Samples had a thickness of approximately 0.1 mm. XAS experiments were performed on three different samples in each S state. In each XAS experiment, measurements were made at two or three orientations, and the same sample was used for measurements at the different orientations.

Data Collection and Analysis. X-ray absorption spectra were collected at the Stanford Synchrotron Radiation Laboratory (SSRL) and at the National Synchrotron Light Source (NSLS). X-ray absorption spectra were measured by monitoring the fluorescence excitation spectrum using a 13-element Ge detector or a Si–Li detector (Jaklevic et al., 1977; Cramer et al., 1988). Sample temperature was maintained at 10 K using an Oxford Instruments CF1204 liquid helium flow cryostat. Simultaneous measurement of the X-ray absorption spectrum of $KMnO_4$ provided the energy calibration (Goodin et al., 1979). EXAFS data were collected on beam line X9-A at the NSLS using either Si(220) or Si(111) double-crystal monochromators with an unfocused beam. XANES data were collected on beam line IV-2 at SSRL using a Si(111) crystal monochromator. The multilayer samples were rotated, and spectra were measured as a function of the angle between the X-ray e-vector and the membrane normal.

Data were treated as previously described (Yachandra et al., 1986; Guiles et al., 1990a). A two-domain spline fit to data from ca. 6600 to 7100 eV was employed for subtraction of a low-frequency background from the data. For a given sample measured at different angles, the EXAFS oscillations were normalized to the same fraction of the edge jump, and identical values were chosen for E_o, the photoionization threshold energy. Uniformity of data analysis was also maintained at other steps, including the transformation of data to k-space.

A square windowing function was applied to the Fourier transforms, and back-transformed data were fit to theoretical phase and amplitude scattering functions calculated using a curved-wave formalism (McKale et al., 1988). Fits were performed on the back-transformed isolates of the first and second Fourier peaks and on the isolates of the second and third Fourier peaks. The EXAFS function, $\chi(k)$, for each orientation was analyzed by curve-fitting to

$$\chi(k) = \sum_{b=1}^{n} \{[N_b F_{ab}(\theta) A_{ab}(k,R_{ab})]/kR_{ab}^2\} \exp(-2\sigma_{ab}^2 k^2) \times \sin(2kR_{ab} + \alpha_{ab}(k,R_{ab})) \quad (1)$$

where $A_{ab}(k,R_{ab})$ and $\alpha_{ab}(k,R_{ab})$ represent the EXAFS amplitude and phase-shift functions, respectively, N_b is the number of b-type backscattering atoms at a mean distance R_{ab} from the absorber atom a, and $k = [(2m_e/h^2)(E-E_o)]^{1/2}$, in which m_e is the electron mass and h is Planck's constant. The damping effect caused by static and thermal disorder is expressed by σ, the Debye–Waller factor.

$F_{ab}(\theta)$ is given by eq 5 below. Fits to eq 1 were done for back-transformed isolates by varying the four parameters R_{ab}, N_b, $-2\sigma^2$, and ΔE_o. The quality of the fit in k-space, or the R-factor, was determined according to the guidelines established by the Sixth International Conference on X-ray Absorption Fine Structure (Bunker et al., 1991) and described by Binsted et al. (1992):

$$R\ (\%) = \sum_{i}^{N} (1/\sigma_i)(|\chi^{exptl}(k_i) - \chi^{theor}(k_i)|)100 \quad (2)$$

where N is the number of data points, and σ_i is defined as

$$1/\sigma_i = k_i^3 \sum_{j}^{N} k_j^3 |\chi^{exptl}(k_j)| \quad (3)$$

An R-factor of 20 is considered a good fit and 40 a poor fit. The function, ϵ^2, is an absolute goodness of fit that takes into account the degree of overdeterminancy in the system:

$$\epsilon^2 = [1/(N_i - p)](N_i/N) \sum_{i}^{N} (1/\sigma_i^2)(\chi^{exptl}(k_i) - \chi^{theor}(k_i))^2 \quad (4)$$

Here N_i is the number of independent parameters, $2\Delta k \Delta R/\pi$, where Δk is the k-range of the data used and ΔR is the width of the window of the Fourier-filtered peak, and p is the number of fit parameters. Because of the dependence of ϵ^2 on the number of parameters, it will vary depending on the number of parameters that have been fixed in a given fit.

Representative fits were chosen after analysis of the following different fit methods. The data were windowed and fit either as pairs of Fourier transform peaks [i.e., peaks I and II ($0.3 \leq R' \leq 3.0$ Å) or peaks II and III ($1.8 \leq R' \leq 4$ Å)] or as isolated peaks [peak II ($1.8 \leq R' \leq 3.0$ Å) or peak III ($2.5 \leq R' \leq 3.5$ Å)]. This method was chosen to avoid potential artifacts introduced by the windowing function (Zhang et al., 1988) and to reduce the correlation between fitting parameters by providing comparisons between multiple combinations of data. Using this method of analysis, best fit values at each orientation were determined.

$F_{ab}(\theta)$ describes the angle dependence of the EXAFS amplitude, which is approximately proportional to $\cos^2 \beta$, where β represents the angle between the X-ray electric field vector e and the absorber–backscatterer vector. Because bound-state dipole-allowed transitions are predominantly of p character, they exhibit a similar angle dependence in which β is defined as the angle between the p-orbital axis and the X-ray e-vector (Smith et al., 1985). If we assume a Gaussian distribution of orientations for the sample disorder, $F_{ab}(\theta)$ can be expressed as

$$F_{ab}(\theta) = 3[\int_{\phi=0}^{\pi}(^1/_2 \sin^2\theta \sin^2\phi + \cos^2\theta \cos^2\phi)P(\phi)\, d\phi]/\int_{\phi=0}^{\pi} P(\phi)\, d\phi \quad (5)$$

where $P(\phi) = \sin\phi \exp[-(\ln 2)(\phi - \phi_{ab})^2/\Omega^2]$, ϕ_{ab} is the angle between the membrane normal and the absorber–backscatter vector sampled over a range of ϕ, and θ is the angle between the X-ray e-vector and the membrane normal. Ω represents the sample disorder or the mosaic spread, which was determined to be about 20–25°. The mosaic spread is determined by comparison of the g_y and g_z peaks of the Cyt b_{559} EPR spectra taken at 15° intervals with the analogous EPR simulations (Blum et al., 1978). Fitting the θ dependence of the amplitude ($F_{ab}(\theta)N_b$) using eq 5 gives values for the average number of backscatterers N_b and the average orientation $\langle\phi_{ab}\rangle$ for a particular backscattering vector. Fits of the θ dependence were done using a mosaic spread of 20–25°, for which we found very little variation in the angle. For example, for the data on the S_1 state, the average angle for the second peak was determined to be 60.2° ± 7° using a mosaic spread of 25° and 60.2° ± 6° using a mosaic spread of 20°. The larger of the two errors is reported.

RESULTS AND DISCUSSION

The degree of orientation in the dried multilayer samples from spinach was established by examination of PS II EPR signals, which exhibit characteristic signal amplitude dependence with orientation (Rutherford, 1985). Figure 1 depicts a typical Cyt b_{559}^+ EPR spectrum obtained from the samples with the membrane normal oriented at 0° or 90° with respect to the magnetic field. The $g_z = 2.97$ feature exhibits maximum intensity when the membrane normal is oriented perpendicular to the magnetic field, and the $g_y = 2.22$ feature is maximal when the membrane normal is oriented parallel to the magnetic field. This angle dependence of the amplitude is consistent with earlier observations (Rutherford, 1985). Simulation of this signal results in an estimate of 20–25° for the mosaic spread of these preparations (Blum et al., 1978). After drying the samples, their activity was assayed by monitoring the amount of Mn multiline EPR signal formed upon illumination at 195 K. The amplitude of the Mn signal was 95–100% of that obtained from randomly oriented membranes of similar concentration that had not been dried. Thus, these samples do not appear to exhibit any appreciable loss of activity as a result of the method used for orientation.

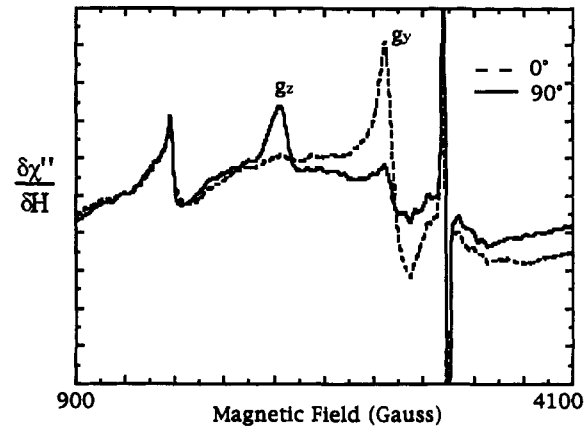

FIGURE 1: EPR spectrum of the cytochrome b_{559}^+ signal present in the dark in oriented PS II membrane particles. The sample was oriented with the membrane normal at 0° or 90° with respect to the magnetic field. EPR conditions were as follows: temperature, 20 K; microwave power, 30 mW; modulation amplitude, 32 G; frequency, 9.215 GHz.

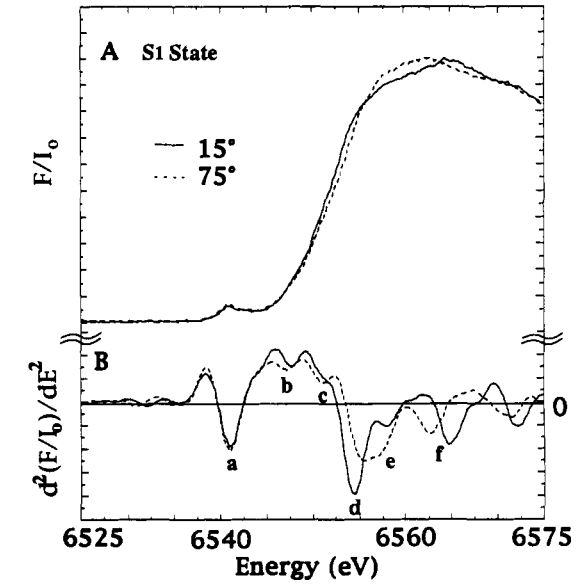

FIGURE 2: (A) S_1-state Mn K-edge X-ray spectra of oriented PS II particles. (B) Second derivatives of the spectra shown in A. The membrane normal was oriented at 15° or 75° with respect to the X-ray e-vector during data acquisition. Second-derivative spectra were generated by analytical differentiation of a polynomial fit to the data over an interval of ±2.5 eV on each side of a data point. Features labeled b–f exhibit clear variations with orientation.

Mn K-Edge Spectra

X-ray absorption Mn K-edge spectra of the preparations in the S_1 state are shown in Figure 2A. Data are shown for two orientations in which the membrane normal is oriented at either 15° or 75° with respect to the polarization direction of the X-rays. The shape of the edge is very different for the two orientations, and several features exhibit a marked angle dependence. The most noticeable features in the K-edge spectra are a peak at 6563 eV, which is greater at θ = 75°, and one at 6565 eV, which is more intense at θ = 15°. These features occur in the region labeled f in the second-derivative spectrum (Figure 2B). Other features in the edge spectra also exhibit dichroism, which is most clearly resolved in the second derivative. Features labeled b (6547 eV), c (6551 eV), d (6554 eV at 15°, 6555.5 at 75°), e (6558 eV), and f

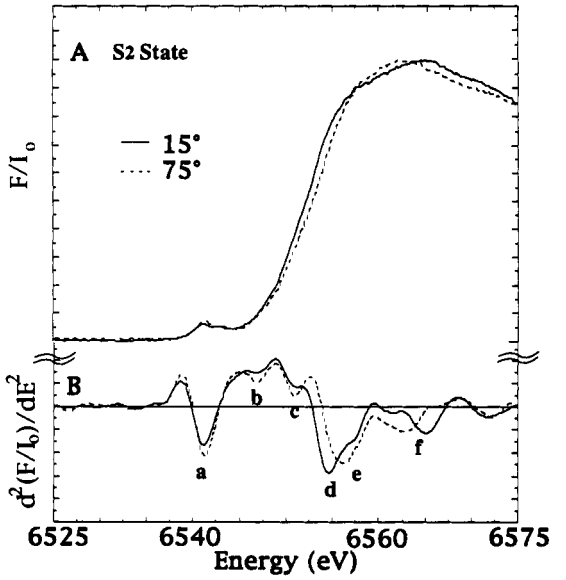

FIGURE 3: (A) S_2-state Mn K-edge spectra of oriented PS II particles. (B) Second derivatives of the spectra shown in A. The indicated angle is that between the membrane normal and the X-ray e-vector. Second derivatives were derived as described in the legend to Figure 2B.

(6565 eV at 75°, 6563 eV at 15°) particularly display clear variations with orientation. Data taken with the membrane normal at 45° give a spectrum intermediate between the two extremes (data not shown).

The pre-edge feature (1s → 3d transition) at 6540.2 eV exhibits some angle dependence. This angle dependence is observable both in the K-edge spectra (Figure 2A) and in the second derivatives of the K-edge spectra (Figure 2B). Although this transition is formally dipole-forbidden, it gains intensity through mixing of the 3d and 4p levels (Shulman et al., 1976). The relatively weak intensity of this transition in the PS II Mn K-edge spectra clearly supports a centrosymmetric hexacoordinate geometry (Roe et al., 1984).

Mn K-edge spectra have also been obtained for PS II membranes in the S_2 state (Figure 3) oriented at either 15° or 75°. These spectra closely resemble the S_1-state K-edge spectra (Figure 2). As for the S_1 state, data taken with θ = 45° are intermediate between the two extremes (data not shown). The K-edge second-derivative spectra accentuate subtle differences between the S_1 and S_2 states. Features d and e exhibit the largest changes as a consequence of advance to the S_2 state; d and e exhibit a smaller degree of dichroism in the S_2 state than in the S_1 state, while for b the dichroism changes only slightly. At each orientation, a comparison of the first derivatives (not shown) of the S_1 and S_2 K-edge spectra reveals that the inflection point energy increases by ~1 eV upon the S_1 to S_2 transition. The overall shapes and inflection point edge energies correlate well with those previously reported for randomly oriented samples (Ono et al., 1992; Yachandra et al., 1987).

Photosystem II EXAFS Fourier Transforms and EXAFS Curve-Fitting

S_1 State. EXAFS and the corresponding Fourier transforms for PS II preparations oriented with the membrane normal at 15° and 75° are shown in Figures 4 (top) and 5A. Measurements were also made at other angles, and these are included in the analyses of the average vector angles and numbers of backscatterers. The Fourier transforms exhibit three well-defined peaks, with maxima occurring close to *R'*

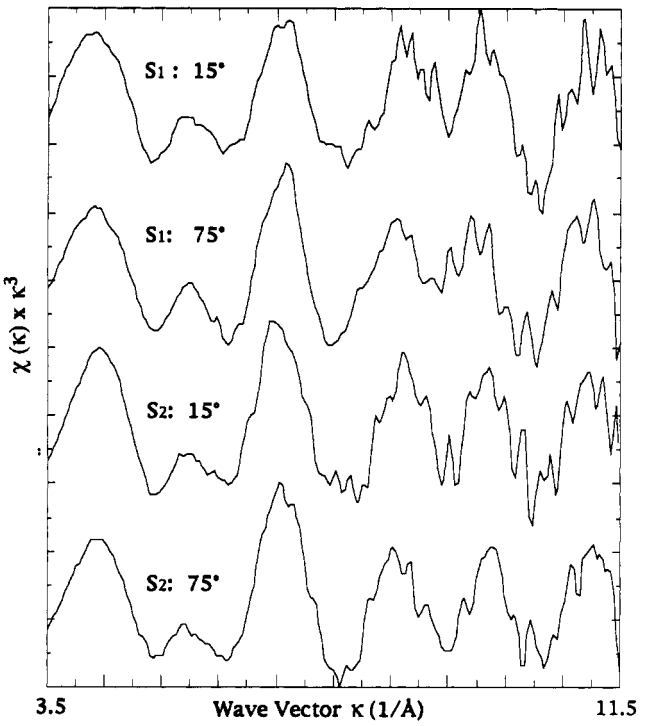

FIGURE 4: *k*-space Mn EXAFS of oriented PSII membrane preparations. The extreme orientations (15° and 75°) for samples poised in the S_1 and S_2 states are shown. Orientation with respect to the X-ray e-vector is as described in the legend to Figure 2. Data are weighted by k^3.

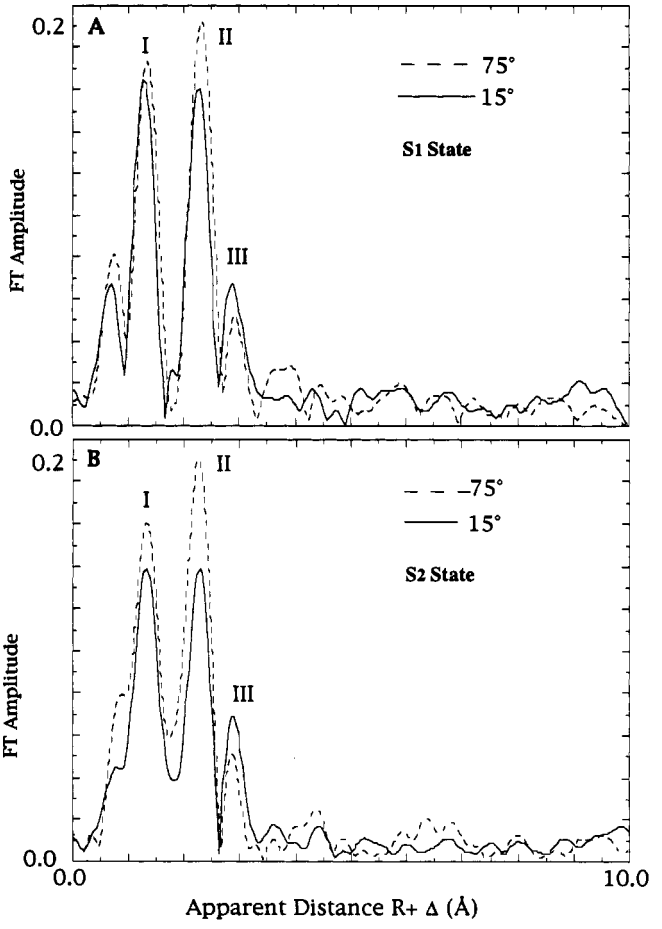

FIGURE 5: Mn EXAFS Fourier transforms of oriented PS II membrane particles: membrane normal oriented at 15° (—) and 75° (– –) with respect to the X-ray e-vector. (A) Dark-adapted samples in the S_1 state. (B) 195 K illuminated samples poised in the S_2 state. All spectra are plotted on the same scale.

Table 1: Mn EXAFS Curve-Fitting Parameters for Oriented PS II Membrane Preparations in the Dark-Adapted S_1 State[a]

angle[b] (deg)	R (Å)	$F(\theta)N_b$	$2\sigma^2$ (Å^2)	R-factor[d]	$\epsilon^2 \times 10^5$ [e]
		First Peak (First Shell)			
15	1.84	2.4	0.002	25.23	1.87
75	1.86	2.3	0.002	16.42	0.95
		First Peak (Second Shell)			
15	1.96	4.2	0.01	25.23	1.87
75	1.96	3.4	0.01	16.42	0.95
		Second Peak			
15	2.71	0.92	0.005	19.13	0.45
15	2.70	0.72	0.002	15.89	0.42
45	2.71	0.96	0.002	25.51	1.10
54.7[c]	2.74	1.20	0.005	14.75	0.30
54.7[c]	2.74	1.16	0.005	14.78	0.42
75	2.73	1.08	0.005	15.96	0.42
75	2.75	1.22	0.005	16.33	0.43
		Third Peak			
15	3.40	0.48	0.005	15.89	0.42
15	3.40	0.54	0.006	20.95	0.96
45	3.41	0.32	0.005	25.51	1.10
45	3.41	0.42	0.005	18.26	0.54
54.7[c]	3.39	0.46	0.005	14.75	0.30
54.7[c]	3.39	0.52	0.005	12.33	0.21
75	3.35	0.36	0.005	15.96	0.42
75	3.35	0.36	0.005	15.97	0.70

[a] Multiple entries at a given angle refer to separate samples. Values for the first peak are averaged from several samples. [b] Angle between the membrane normal and the X-ray electric field vector. [c] Mean values for isotropic S_1-state samples. The EXAFS data of isotropic samples should be identical to the data of oriented samples recorded with an angle of 54.7°. [d] R-factors from eq 2 in Materials and Methods fits. [e] See eq 4 in Materials and Methods for definition.

= 1.3, 2.3, and 2.9 Å. The transforms show clear differences with the orientation of the sample, and angle-dependent changes in the Fourier transform amplitudes are observable for all three peaks. The intensities of both peaks I and II are greater at $\theta = 75°$, while peak III is more intense at $\theta = 15°$. These changes are reproducible and independent of background removal, and the trends are similar to those previously reported for whole chloroplasts (George et al., 1989), but the data are quite different.

(1) Peak I. The first Fourier peak (peak I) is best described by two shells of Mn–O(N) occurring at 1.83–1.86 and 1.93–2.05 Å (see Table 1). EXAFS cannot discriminate between scatterers of similar atomic number because their backscattering amplitudes and phase shifts are similar; thus, N and O cannot be distinguished.

The first shell of scatterers is best modeled by two low-Z scatterers at about 1.85 Å from each Mn atom. In previous work (DeRose et al., 1994; DeRose, 1990; McDermott et al., 1988; Yachandra et al., 1987), this shell was assigned to bridging O atoms. This assignment was based on the observed bridging distance for O atoms in μ_2- and μ_3-oxo-bridged multinuclear Mn clusters, which is typically 1.8–1.9 Å (Wieghardt, 1989; Pecoraro, 1992).

In the fits of the first two Fourier peaks (as described in Materials and Methods), the fit error decreases by a factor of at least 2 when the second shell of light scatterers is included. This supports the requirement of the two shells. This second shell of O or N scatterers can be fit with either a small number of scatterers ($N_b = 0.4$) or a relatively large Debye–Waller factor ($\sigma^2 = -0.02$ Å^2), which is indicative that the scatterers are disordered. The number of scatterers and the Debye–Waller factor are highly correlated, and an increase in σ^2 can attenuate the entire EXAFS and require an increase in N as well (Teo, 1986). Using large Debye–Waller factors, an approximate coordination number of 3–5 is determined from

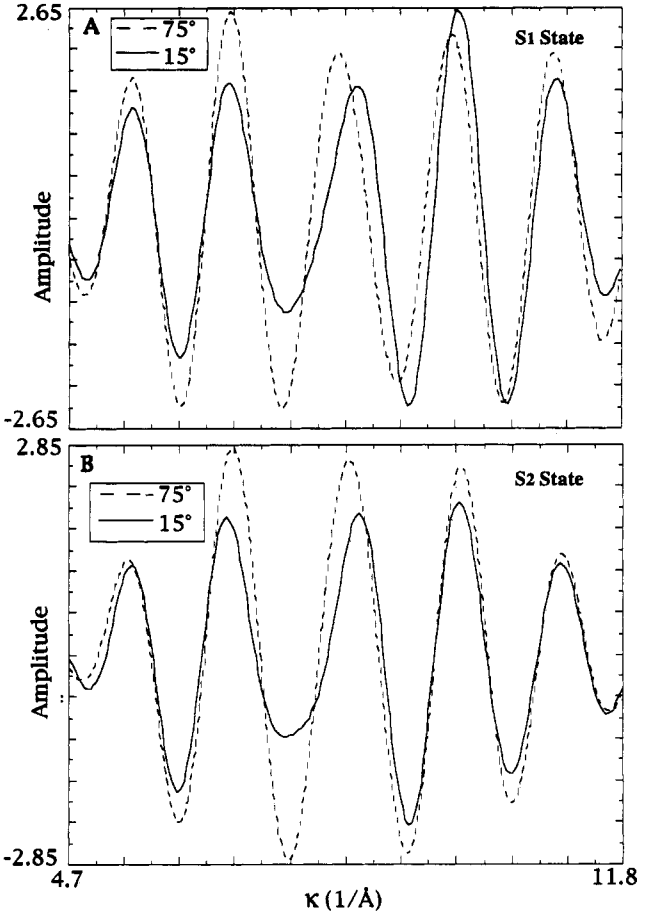

FIGURE 6: Fourier isolates of peaks II and III in the Fourier transforms: samples oriented at $\theta = 15°$ (—) and 75° (– –). Clear variations in the amplitudes of the oscillations are observed for the two extreme orientations: (A) S_1 state; (B) S_2 state.

the fits at all orientations. The two-shell fit for the first Fourier peak is consistent with other studies on randomly oriented preparations (Corrie et al., 1990; DeRose et al., 1994; DeRose, 1990; MacLachlan et al., 1992; McDermott et al., 1988; Yachandra et al., 1987).

(2) Peak II. Fits of the second Fourier peak were done in conjunction with either the first or the third Fourier peak, as well as alone when the data permitted good peak isolation. The back-transformed isolates of peaks II and III are shown in Figure 6A. The large differences in the amplitude and beat pattern of the oscillations at the two orientations reflect the dichroism observed in the Fourier transform (FT) amplitudes. The quality of the fits is judged using the fit error as defined in the Materials and Methods section; this parameter reflects the deviations between the simulations and the isolates. Both types of fit require a shell of heavy atom scatterers (Mn) at about 2.72 Å (see Table 1). Figure 7A depicts the polar plots of the amplitudes, $F_{ab}(\theta)N_b$, of this Mn–Mn interaction. By fitting the angle dependence of the amplitude to eq 5, the approximate number of backscatterers and the average orientation for that shell of scatterers can be determined (see Table 2). The 2.72-Å Mn–Mn EXAFS peak corresponds to 1.1 ± 0.1 interactions per Mn at an angle of $\langle\phi\rangle = 60° \pm 7°$, with respect to the membrane normal. The number of Mn–Mn interactions implies at least two 2.7-Å vectors for the OEC; thus, this angle represents an average value. An average angle of 60° is consistent with those of the two resolved vectors found in oriented ammonia-treated PS II particles (H. Dau, personal communication). The average distance and number of backscatterers (Table 2) are in good

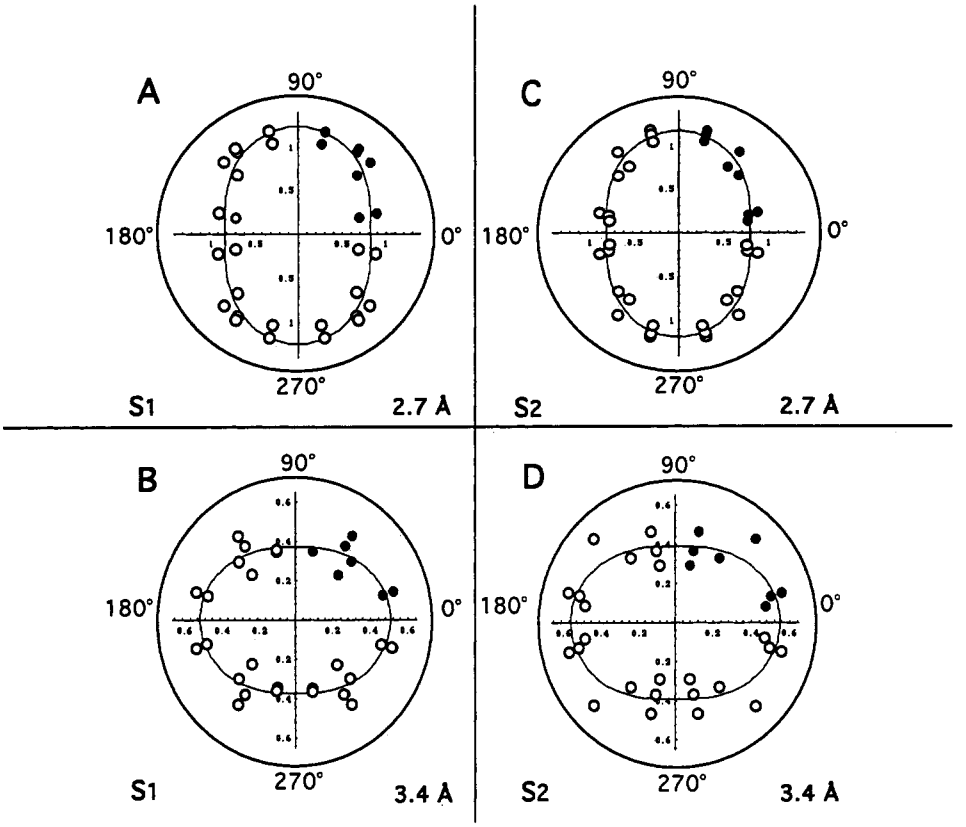

FIGURE 7: Polar plots of the orientation dependence of the apparent number, $F_{sb}(\theta)N_b$, of the interactions derived from curve-fitting of the Fourier isolates as shown in Figure 6. Plots are best fits to eq 5 for (A) S_1, 2.7-Å Mn–Mn; (B) S_1, 3.4-Å Mn–Mn; (C) S_2, 2.7-Å Mn–Mn; and (D) S_2, 3.4-Å Mn–Mn. Plotted points (10°, 15°, 45°, and 75°) arise from three different data sets on oriented PS II membrane particles. The data point at 54.7° is taken from EXAFS data for a randomly oriented preparation. Solid points are data, and open circles are data points that have been mirrored for clarity. The resulting isotropic coordination numbers and average angles with respect to the membrane normal are listed in Table 2.

Table 2: Average Number of Backscatterers per Mn Atom and Orientation to the Membrane Normal Determined from Polar Plots (Figure 7) Using Equation 5

R (Å)	N_b	$\langle\phi\rangle$ (deg)
	S_1 State	
2.72 ± 0.03	1.1 ± 0.1	60 ± 7
3.38 ± 0.03	0.42 ± 0.08	43 ± 11
	S_2 State	
2.71 ± 0.01	1.0 ± 0.1	60 ± 4
3.35 ± 0.05	0.44 ± 0.07	43 ± 10

agreement with data from randomly oriented samples (DeRose et al., 1994; DeRose, 1990; McDermott et al., 1988; Yachandra et al., 1987). From work on several multinuclear Mn(III) and Mn(IV) complexes, this distance is characteristic of μ_2-oxo-bridged or μ_3-oxo-bridged Mn clusters (Wieghardt, 1989; Pecoraro, 1992; Plaskin et al., 1972; Stebler et al., 1986). Additionally, the determined orientation of the 2.7-Å Mn–Mn vector with respect to the membrane normal agrees, within error, with the orientation determined by George and coworkers (1989) for oriented whole chloroplasts, although they found 2.1 ± 0.8 interactions for this vector.

From previous studies on randomly oriented PS II preparations (DeRose et al., 1994; DeRose, 1990), it has been observed that the second shell of Mn–O(N) scatterers is highly disordered, which is consistent with the relatively high Debye–Waller values used for fitting in this study. Therefore, the amplitude dependence of the first peak in the Fourier transform as a function of the angle can be correlated qualitatively with that of the bridging ligands. In our work on randomly oriented PS II preparations, however, we have determined that the second Mn–O(N) shell makes only a small contribution to the EXAFS spectrum and the ensuing Fourier transforms. If we assume that the first shell of Mn–O/N scatterers makes the main contribution to the first peak, the amplitude dependence of the first peak in the Fourier transform as a function of the angle can be correlated qualitatively with that of the bridging ligands. Due to the large number of Mn–O/N interactions in the OEC, it is difficult to make a quantitative determination for the first peak. The first Fourier peak exhibits an angle dependence similar to that of the second Fourier peak, both of which are greater at 75° than at 15°. This similarity in angle dependence implies that the orientation of the average Mn–O vector is comparable to that of the Mn–Mn 2.7-Å vector, which is consistent with the assignment of the first shell of light scatterers to bridging ligands in a μ_2-oxo geometry. Because the first peak would exhibit no significant dichroism if the Mn_2O_2 di-μ-oxo plane were perpendicular to the membrane plane, we can rule out this configuration for at least one of the Mn_2O_2 moieties.

Interestingly, the apparent length for the Mn–Mn interaction varies with θ, the orientation of the membrane normal with respect to the polarization of the incoming X-ray beam. The apparent distance is 0.03–0.04 Å longer (2.73–2.75 Å) at an orientation of 75° than at 15° (2.70–2.71 Å). Although this difference is small, it is reproducible and was also reported in data on whole chloroplasts (George et al., 1989). Because the phase and amplitude functions should be identical for the interaction, the difference in length appears to be significant. The EXAFS represents an average of similar interactions with distinct angle and distance dependencies. At a given θ value, the spectra can emphasize different interactions, depending on the angle with respect to the e-vector, leading

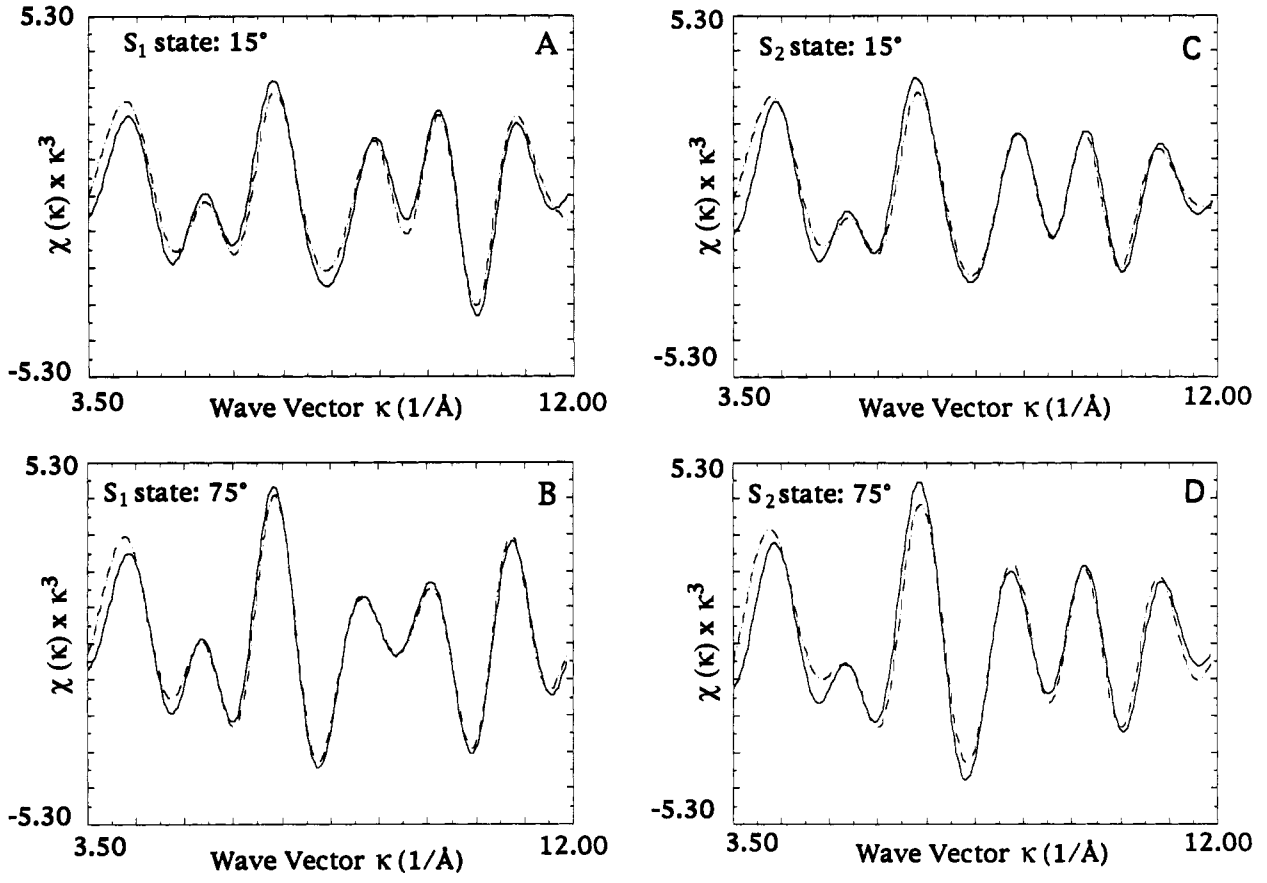

FIGURE 8: Simulations (- · -) of Fourier transform peaks I, II, and III plotted over the back-transformed isolate (—) of those three peaks. Samples were oriented at $\theta = 15°$ and 75°. Fit simulations were generated as described in the text: (A) S_1 state, 15°; (B) S_1 state, 75°; (C) S_2 state, 15°; (D) S_2 state, 75°.

to the determination of a greater length. Thus, the dependence of R_{ab} on θ provides information regarding the angle distribution of interaction lengths about the active site. A recently proposed model for the OEC in the S_1 state (Yachandra et al., 1993) consists of two di-μ-oxo-bridged binuclear centers in which one center is in the Mn(III)–Mn(III) oxidation state and the other is in the Mn(IV)–Mn(IV) oxidation state, leading to different lengths for the Mn–Mn interaction. The variation in R_{ab} with angle could possibly result from a better selectivity for the Mn(III)–Mn(III) di-μ-oxo-bridged binuclear center at $\theta = 75°$ and for the Mn(IV)–Mn(IV) di-μ-oxo-bridged binuclear center at $\theta = 15°$.

(3) Peak III. Curve-fitting of the Fourier transform isolates of the second and third Fourier peaks or only the third peak reveals that the inclusion of a Mn–Mn interaction at 3.38 Å best fits the data (see Table 1). Both EPR (Boussac et al., 1989; Sivaraja et al., 1989; Ono et al., 1991) and EXAFS data (Yachandra et al., 1993) of Sr^{2+}-replaced PS II particles suggest that Ca^{2+} is situated close to the Mn cluster. The inclusion of Mn–Ca or Mn–C improves the quality of the fit; however, the degree of improvement does not warrant the inclusion of another shell to describe the data, and as such we have limited our analysis to a single Mn–Mn interaction at ~3.38 Å. However, this does not preclude the possibility of the presence of Ca or C at about 3.4 Å. Figure 7B depicts polar plots of the amplitude dependence for this Mn–Mn interaction. Using eq 5, these data are best described by 0.42 ± 0.08 interaction per Mn, corresponding to a vector with an angle of $\langle\phi\rangle = 43° \pm 11°$ with respect to the membrane normal (Table 2). From model compound studies, Mn–Mn distances of 3.4 Å have been observed in complexes with either a single μ_2-oxo bridge between the two Mn atoms or two μ_2-carboxylato bridges and one μ_2-oxo bridge (Vincent et al., 1987; Wieghardt et al., 1983, 1985; Sheats et al., 1987).

The approximate number of backscatterers and the distance are in good agreement with what has been reported for randomly oriented PS II particles (Yachandra et al., 1993; DeRose et al., 1994; DeRose, 1990). The orientation of this vector, however, contrasts greatly with the 0° orientation reported for whole chloroplasts (George et al., 1989). The $\langle\phi\rangle = 0°$ orientation for the 3.4-Å vector determined by George et al. (1989) results from the fact that a Fourier transform peak at 3.4 Å was not observed for $\theta = 90°$. It is possible, however, that the amplitude of that peak was non-zero, but was within the noise level of the data and therefore not observable. The difficulties in fitting a peak of such small amplitude could lead to the discrepancies in the angle determination. Recent work on oriented multilayer preparations of ammonia-treated PSII particles gives a ~30° orientation for the 3.4-Å vector with respect to the membrane normal (H. Dau, personal communication). If we allow for error limits and possible differences due to ammonia treatment, this orientation is consistent with the present data. Additionally, for $\theta = 45°$, George et al. (1989) observed a peak at an apparent distance of $R + \Delta = 3.8$ Å, which they attributed to a multiple scattering process. We do not observe any peaks at that radial distance for $\theta = 45°$ (data not shown) or any peaks that do not exhibit a $\cos^2\beta$ dependence. Our data also contrast with an XAS study of unoriented PS II particles done by MacLachlan and co-workers (1992), which reports a Mn–Ca interaction at 3.8 Å. The differences between the two studies could arise from the fact that MacLachlan et al. (1992) prepared the PS II particles in the absence of Ca^{2+}, while the samples used in this study were prepared in the

Table 3: Mn EXAFS Curve-Fitting Parameters for Oriented PS II Membrane Preparations in the 190 K Illuminated S_2 State[a]

angle[b] (deg)	R (Å)	$F(\theta)N_b$	$2\sigma^2$ (Å^2)	R-factor[d]	$\epsilon^2 \times 10^5$ [e]
		First Peak (First Shell)			
15	1.83	2.2	0.005	18.65	1.16
75	1.84	3.2	0.008	22.95	1.37
		First Peak (Second Shell)			
15	1.93	3.9	0.01	18.65	1.16
75	1.94	4.4	0.01	22.95	1.37
		Second Peak			
10	2.71	0.78	0.003	32.77	0.60
15	2.70	0.90	0.006	30.25	1.20
15	2.70	0.80	0.005	28.68	0.76
45	2.71	0.94	0.005	21.48	1.77
54.7[c]	2.72	0.94	0.003	27.31	0.46
75	2.70	1.10	0.005	25.69	1.35
75	2.71	1.22	0.005	20.18	2.38
		Third Peak			
10	3.30	0.48	0.003	22.19	0.76
15	3.33	0.58	0.006	22.27	1.12
45	3.37	0.60	0.003	23.36	1.20
54.7[c]	3.34	0.40	0.005	19.60	0.70
75	3.40	0.48	0.005	29.35	1.98
75	3.40	0.30	0.005	14.16	0.97
75	3.32	0.38	0.008	14.19	2.65

[a] Multiple entries at a given angle refer to separate samples. Values for the first peak are averaged from several samples. [b] Angle between the membrane normal and the X-ray electric field vector. [c] Mean values for isotropic S_2-state samples. The EXAFS data of isotropic samples should be identical to the data of oriented samples recorded with an angle of 54.7°. [d] R-factors from eq 2 in Materials and Methods fits. [e] See eq 4 in Materials and Methods for definition.

presence of 5 mM Ca^{2+}. The absence of Ca^{2+} during preparation could result in a perturbation of the Ca^{2+} binding site, leading to the observance of a Mn interaction at longer distances.

Figure 8 depicts simulations of the back-transformed isolates of the three Fourier peaks for both the S_1 (A and B) and S_2 (C and D) states. The fit parameters (see Tables 1 and 3) used for the simulations are derived from the two separate types of fits that were performed: (1) Fourier peaks I and II together and (2) Fourier peaks II and III together. The best fit parameters from these fits were combined to construct a simulation of the back-transform of the three Fourier peaks. These constructed simulations demonstrate the excellent agreement between the fit parameters shown in Tables 1 and 3 and those of the back-transformed isolates of the three Fourier peaks. Thus, these simulations, obtained using a four-shell model of two shells of low-Z scatterers at $R < 2.0$ Å and Mn–Mn interactions at 2.7 and 3.4 Å, respectively, adequately describe the three Fourier transform peaks generated from the EXAFS of the OEC.

S_2 State. The EXAFS and Fourier transforms of PS II particles poised in the S_2 state are shown in Figures 4 (bottom) and 5B, respectively. The amplitude of the Fourier peaks exhibits an angle dependence similar to that observed for the S_1 state; peaks I and II are greater at $\theta = 15°$, and the amplitude of peak III is greater at $\theta = 75°$. The peaks occur at approximately the same radial distances detected in the S_1 state. The back-transformed isolates of Fourier peaks II and III (Figure 6B) show trends with respect to orientation similar to those observed for the S_1 state. However, a comparison of the S_2 isolates at two orientations shows that the spectra are somewhat different. Clear differences exist in the amplitude and frequency of the k-space oscillations for 15° and 75° orientations, which can be correlated with the observed dichroism in the amplitude of the Fourier transforms. For

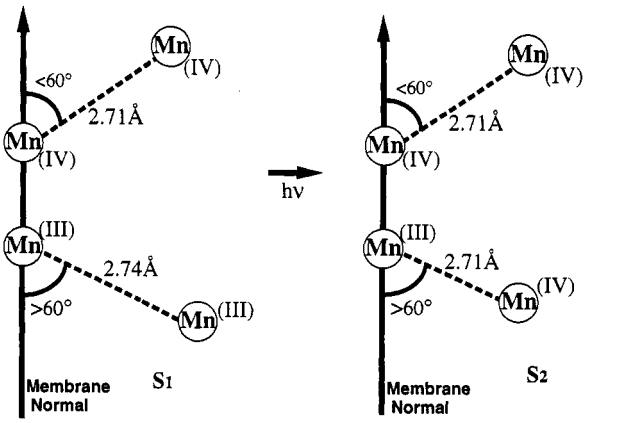

FIGURE 9: Proposed model for the change in length of the Mn–Mn vector greater than 60°, upon the S_1 to S_2 transition.

the two states, best fit parameters yield similar values with one exception (see Table 3). In the S_2 state the distance of the 2.70-Å Mn–Mn vector for $\theta = 75°$ decreases by 0.03–0.04 Å relative to that of the S_1 state. A decrease in bond length and the ~1-eV shift of the Mn K-edge inflection point to higher energy upon cryogenic advance to the S_2 state provide supportive evidence for Mn(III) oxidation to Mn(IV).

The decrease in the length of the 2.7-Å Mn–Mn vector upon the S_1 to S_2 transition shows up only at 75°, but not at the smaller angle of 15°. Of the two 2.7-Å vectors that have been resolved in other studies (Liang et al., 1994; De Rose et al., 1994; Guiles et al., 1990b; H. Dau, personal communication), it appears that a Mn atom in the vector having the greater angle to the membrane normal undergoes oxidation. We propose that the asymmetry of the S_1 state can be resolved into a shorter (2.71 Å) Mn(IV)–Mn(IV) vector, which forms an angle of less than 60° to the membrane normal, and a longer (≥2.74 Å) Mn(III)–Mn(III) vector, which forms an angle of greater than 60° to the membrane normal (see Figure 9). We speculate that the Mn(III)–Mn(III) dimer associated with this longer vector is oxidized to Mn(III)–Mn(IV) on the S_1 to S_2 transition.

Not many model compounds are available with which to make comparisons, but from a review of model compounds (Wieghardt, 1989), we can compare some Mn(III)–Mn(III) dimers with Mn(III)–Mn(IV) dimers. The ligands are not the same for these compounds and not all have di-μ-oxo-bridge core structures (some are dihydroxy or have μ_3-oxo bridges), but the general trend is that Mn(III)–Mn(III) dimers were found to have Mn–Mn vector lengths that were longer than those for most Mn(III)–Mn(IV) dimers. These data from model compounds support our proposal that oxidation of the Mn complex in the S_2 state leads to a shorter Mn vector length in one dimer.

Figure 10 depicts Fourier isolates of peaks I, II, and III for S_1 and S_2 at 15° (A) and at 75° (B). The changes that occur upon the S_1 to S_2 transition are much more apparent at 75° than at 15°, especially in the 9–11-Å^{-1} region. This is also supportive of a model in which changes occur in the vector closer to 75° upon the S_1 to S_2 advance. Polar plots depicted in Figure 7 (C and D) allow the determination of both the orientation of the Mn vectors with respect to the membrane and the average coordination number. For the 2.70-Å Mn–Mn vector, the average coordination number is 1.0 ± 0.1, and the average orientation of the vector with respect to the membrane normal is $\langle\phi\rangle = 60° \pm 4°$. The 3.4-Å vector makes an angle of 43° ± 10° with respect to the membrane normal and has an average coordination number of 0.44 ± 0.07. For

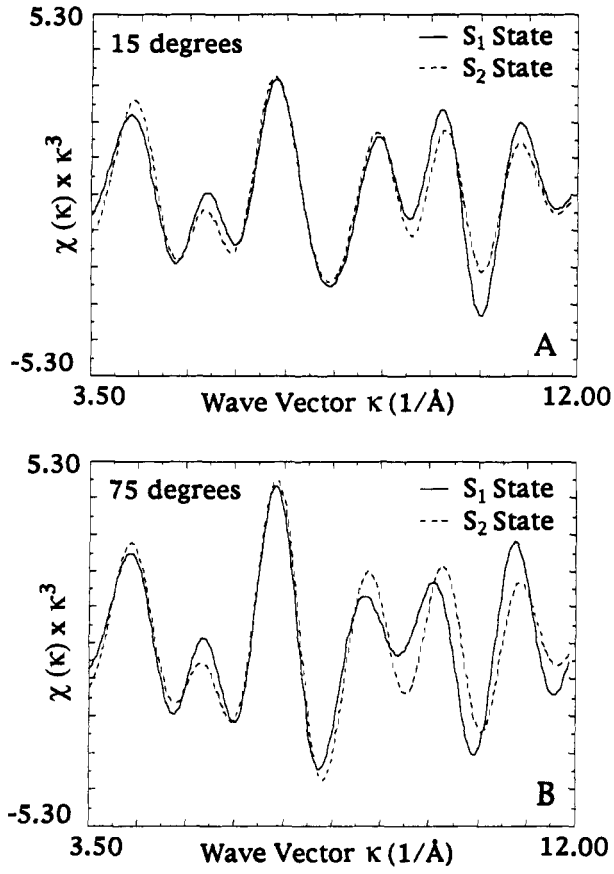

FIGURE 10: Isolates of Fourier peaks I, II, and III shown for S_1 (—) vs S_2 (– –): (A) 15°; (B) 75°.

the two Mn–Mn vectors, the determined values of coordination numbers and $\langle\phi\rangle$ for the S_1 and S_2 states concur within error. The similarity in dichroism for both the edge spectra and the Fourier transform amplitudes suggests that the overall structure and symmetry of the OEC are conserved in the first two S states of the Kok cycle. On the basis of previous results from unoriented preparations, this overall conservation of structure is expected (DeRose et al., 1994; DeRose, 1990; McDermott et al., 1988; Yachandra et al., 1987).

SUMMARY

Mn K-edge spectra and EXAFS of oriented PS II particles poised in the S_1 and S_2 states are highly dichroic, revealing that the OEC is asymmetric with respect to the membrane normal. Structural features determined from the EXAFS agree well with previously reported results on randomly oriented PS II particles. Specific features of the complex include Mn–O interactions at about 1.84 and 1.95 Å and a Mn–Mn distance of 2.72 Å, which makes an angle of 60° ± 7° with the membrane normal. An additional Mn–Mn vector at 3.38 Å, oriented at 43° ± 10° to the membrane normal, is also resolved. These structural characteristics and the symmetry of the complex remain relatively invariant upon advance to the S_2 state, indicating that no large structural changes are occurring. We have some evidence for the occurrence of a minor structural change, and that will need to be addressed in a future paper. Mn K-edge data reveal an ~1-eV shift of inflection point energy at each orientation upon S_1 to S_2 state transformation, consistent with the putative oxidation of the Mn cluster.

From the XAS measurements on oriented PS II membrane particles, the relative orientation of the OEC within the membrane can be determined. Given the average coordination

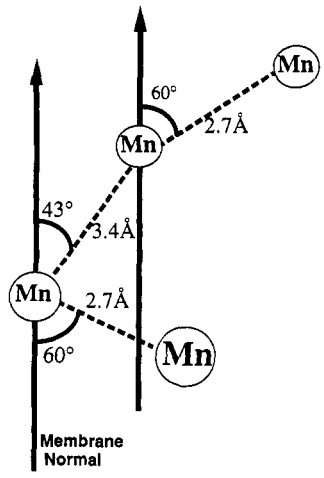

FIGURE 11: Proposed model for the structure of the OEC oriented within the membrane. Note that the vector measurements of 60° and 43° are averages (H. Dau, personal communication).

number and the number of Mn atoms, we suggest that the Mn 2.7-Å interaction arises from two di-μ-oxo-bridged dimers oriented at an average angle of 60° with respect to the membrane normal. The longer bond distance observed at the 75° orientation in the S_1 state suggests that the two dimers are not completely equivalent. More recent work on modified PS II preparations yields two distinct distances for the dimers (Liang et al., 1994; H. Dau, personal communication). Thus, the distances and angles reported for these oriented preparations most probably reflect an average of two discrete vectors. We propose that the two di-μ-oxo-bridged Mn binuclear centers are linked by either a mono-μ-oxo or a mono- or dicarboxylato 3.3–3.4-Å bridge. Our results suggest that this vector is oriented at an angle of 43° with respect to the membrane normal (Figure 11). The reported structural parameters do not uniquely determine the structure for the OEC; other arrangements of the vectors are possible. Another potential structure for the OEC includes a sequential arrangement of the Mn–Mn 2.7-Å vectors, followed by the 3.4-Å vector (DeRose et al., 1994). The average number of Mn backscatterers at 2.7 Å for this model would be 1.0. The vector angles we have found are consistent with both of these models. Each of these vectors transcribes a cone of possible angles about the membrane normal, and the data from this study do not describe only one molecular configuration. The planar model in Figure 11 represents one of several possible configurations. Highly symmetric cubane-like structures, however, can be ruled out by the observed dichroism of the Mn K-edge and EXAFS data.

ACKNOWLEDGMENT

We thank Dr. Stephen P. Cramer for the use of his cryostat and Ge detector and Dr. Britton Chance for the use of his Ge detector. We are grateful to Dr. S. Khalid and Dr. B. Hedman for invaluable assistance at the beam lines. We thank Dr. Holger Dau for his vector-fitting program. We thank Dennis Kim for his assistance with sample preparation and Wenchuan Liang and Melissa Grush for their assistance with XAS data collection. Synchrotron radiation facilities were provided by the Stanford Synchrotron Radiation Laboratory (SSRL) and the National Synchrotron Light Source (NSLS), both supported by DOE. The Biotechnology Laboratory at SSRL and beam line X9-A at NSLS are supported by the National Center for Research Resources of the National Institutes of Health.

REFERENCES

Babcock, G. T., Barry, B. A., Debus, R. J., Hoganson, C. W., Atamian, M., McIntosh, L., Sithole, I., & Yocum, C. F. (1989) *Biochemistry 28*, 9557.

Berthold, D. A., Babcock, G. T., & Yocum, C. F. (1981) *FEBS. Lett. 134*, 231.

Binsted, N., Strange, R. W., & Hasnain, S. S. (1992) *Biochemistry 31*, 12117.

Blum, H., Salerno, J. C., & Leigh, J. S. (1978) *J. Magn. Reson. 30*, 385.

Boussac, A., Zimmermann, J.-L., & Rutherford, A. W. (1989) *Biochemistry 28*, 8984.

Brettel, K, Sieckmann, I., Fromme, P., van der Est, A., & Stehlik, D. (1992) *Biochim. Biophys. Acta 1098*, 266.

Bunker, G., Bunker, B. A., Crozier, D., Goulon, J., Gurman, S. J., Hasnain, S. S., Heald, S. M., Koningsberger, D. C., Natoli, R., Rehr, J. R., Sayers, D., & Udagawa, Y. (1991) *X-ray Absorption Fine Structure* (Hasnain, S. S., Ed.) p 751, Ellis Horwood Ltd., Chichester, U.K.

Corrie, A. R., Evans, M. C. W., Hubbard, J. A. M., Strange, R. W., & Hasnain, S. S. (1990) in *Current Research in Photosynthesis* (Baltscheffsky, M., Ed.) Vol. I, p 793, Kluwer Academic Publishers, Dordrecht, The Netherlands.

Cramer, S. P., Tench, O., Yocum, M., & George, G. N. (1988) *Nucl. Instrum. Methods A266*, 586.

Debus, R. J. (1992) *Biochim. Biophys. Acta 1102*, 269.

Deisenhofer, J., Epp, O., Miki, K., Huber, R., & Michel, H. (1985) *Nature 318*, 618.

DeRose, V. J. (1990) Ph.D. Thesis, University of California, Berkeley, CA, Lawrence Berkeley Laboratory Report LBL-30077.

DeRose, V. J., Mukerji, I., Latimer, M. J., Yachandra, V. K., Sauer, K., & Klein, M. P. (1994) *J. Am. Chem. Soc. 116*, 5239.

Dismukes, G. C., & Sauer, K. (1978) *Biochim. Biophys. Acta 504*, 431.

Flank, A. M., Weininger, M., Mortensen, L. E., & Cramer, S. P. (1986) *J. Am. Chem. Soc. 108*, 1049.

George, G. N., Prince, R. C., & Cramer, S. P. (1989) *Science 243*, 789.

George, G. N., Cramer, S. P., Frey, T. G., & Prince, R. C. (1993) *Biochim. Biophys. Acta 1142*, 240.

Goodin, D. B., Falk, K. E., Wydrzynski, T., & Klein, M. P. (1979) 6th Annual Stanford Synchrotron Radiation Laboratory Users Group Meeting, SSRL Report No. 79/05, p 10, SSRL, Stanford, CA.

Guiles, R. D., Yachandra, V. K., McDermott, A. E., Cole, J. L., Dexheimer, S. L., Britt, R. D., Sauer, K., & Klein, M. P. (1990a) *Biochemistry 29*, 486.

Guiles, R. D., Zimmermann, J.-L., McDermott, A. E., Yachandra, V. K., Cole, J., Dexheimer, S. L., Britt, R. D., Wieghardt, K., Bossek, V., Sauer, K., & Klein, M. P. (1990b) *Biochemistry 29*, 471.

Jaklevic, J., Kirby, J. A., Klein, M. P., Robertson, A. S., Brown, G. S., & Eisenberger, P. (1977) *Solid State Commun. 23*, 679.

Klein, M. P., Sauer, K., & Yachandra, V. K. (1993) *Photosynth. Res. 38*, 265.

Kok, B., Forbush, B., & McGloin, M. (1970) *Photochem. Photobiol. 11*, 457.

Liang, W., Latimer, M. J., Dau, H., Roelofs, T. A., Yachandra, V. K., Sauer, K., & Klein, M. P. (1994) *Biochemistry 33*, 4923.

MacLachlan, D. J., Hallahan, B. J., Ruffle, S. V., Nugent, J. H. A., Evans, M. C. W., Strange, R. W., & Hasnain, S. S. (1992) *Biochem. J. 285*, 569.

McDermott, A. E., Yachandra, V. K., Guiles, R. D., Cole, J. L., Dexheimer, S. L., Britt, R. D., Sauer, K., & Klein, M. P. (1988) *Biochemistry 27*, 4021.

McKale, A. G., Veal, B. W., Paulikas, A. P., Chan, S.-K., & Knapp, G. S. (1988) *J. Am. Chem. Soc. 110*, 3763.

Ono, T.-A., Kusunoki, M., Matsushita, T., Oyanagi, H., & Inoue, Y. (1991) *Biochemistry 30*, 6836.

Ono, T.-A., Noguchi, T., Inoue, Y., Kusunoki, M., Matsushita, T., & Oyanagi, H. (1992) *Science 258*, 1335.

Pecoraro, V. L. (1992) in *Manganese Redox Enzymes* (Pecoraro, V. L., Ed.) p 197, VCH Publishers, New York.

Penner-Hahn, J. E., Fronko, R. M., Pecoraro, V. L., Yocum, C. F., Betts, S. D., & Bowlby, N. R. (1990) *J. Am. Chem. Soc. 112*, 2549.

Plaskin, P. M., Stoufer, R. C., Mathew, M., & Palenik, G. J. (1972) *J. Am. Chem. Soc. 94*, 2121.

Prince, R. C., Crowder, M. S., & Bearden, A. J. (1980) *Biochim. Biophys. Acta 592*, 323.

Roe, A. L., Schneider, D. J., Mayer, R. J., Pyrz, J. W., Widom, J., & Que, L., Jr. (1984) *J. Am. Chem. Soc. 106*, 1676.

Rutherford, A. W. (1985) *Biochim. Biophys. Acta 807*, 189.

Sauer, K., Yachandra, V. K., Britt, R. D., & Klein, M. P. (1992) in *Manganese Redox Enzymes* (Pecoraro, V. L., Ed.) p 141, VCH Publishers, New York.

Sheats, J. E., Czernuszewicz, R. S., Dismukes, G. C., Rheingold, A. L., Petrouleas, V., Stubbe, J., Armstrong, W. H., Beer, R. H., & Lippard, S. (1987) *J. Am. Chem. Soc. 109*, 1435.

Shulman, R. G., Yafet, Y., Eisenberger, P., & Blumberg, W. E. (1976) *Proc. Natl. Acad. Sci. U.S.A. 73*, 1384.

Sivaraja, M., Tso, J., & Dismukes, G. C. (1989) *Biochemistry 28*, 9459.

Smith, T. A., Penner-Hahn, J. E., Berding, M. A., Doniach, S., & Hodgson, K. O. (1985) *J. Am. Chem. Soc. 107*, 5945.

Stebler, M., Ludi, A., & Bürgi, H.-B. (1986) *Inorg. Chem. 25*, 4743.

Teo, B. K. (1986) in *EXAFS: Basic Principles and Data Analysis*, Springer Verlag, New York.

Vincent, J. B., Christmas, C., Huffman, J. C., Christou, G., Chang, H.-R., & Hendrickson, D. N. (1987) *J. Chem. Soc., Chem. Commun. 1987*, 236.

Wieghardt, K. (1989) *Angew. Chem., Int. Ed. Engl. 28*, 1153.

Wieghardt, K., Bossek, U., & Gebert, W. (1983) *Angew. Chem., Int. Ed. Engl. 22*, 328.

Wieghardt, K., Bossek, U., Ventur, D., & Weiss, J. (1985) *J. Chem. Soc., Chem. Commun. 1985*, 347.

Yachandra, V. K., Guiles, R. D., McDermott, A. E., Britt, R. D., Dexheimer, S. L., Sauer, K., & Klein, M. P. (1986) *Biochim. Biophys. Acta 850*, 324.

Yachandra, V. K., Guiles, R. D., McDermott, A. E., Cole, J. L., Britt, R. D., Dexheimer, S. L., Sauer, K., & Klein, M. P. (1987) *Biochemistry 26*, 5974.

Yachandra, V. K., DeRose, V. J., Latimer, M. J., Mukerji, I., Sauer, K., & Klein, M. P. (1993) *Science 260*, 675.

Zhang, K., Stern, E. A., Ellis, F., Sanders-Loehr, J., & Shiemke, A. K. (1988) *Biochemistry 27*, 7470.